Granular Matter (2022) 24:86
https://doi.org/10.1007/s10035-022-01244-4

ORIGINAL PAPER

Relation between force chain quantitative characteristics and side wall friction behaviour during ferrous powder compaction

Wei Zhang[1] · Shuai Zhang[1] · Jianjun Tan[1] · Ning Zhang[1] · Bingsan Chen[1]

Received: 27 November 2021 / Accepted: 9 May 2022 / Published online: 16 June 2022

Abstract
The internal mechanical behavior of powder system and the side wall friction behavior during powder compaction keep unclear yet. They are significant for revealing the densification behavior during powder compaction. The evolution of force chain quantitative characteristics (number, length, direction coefficient and buckling degree) and side wall friction characteristics (nominal friction coefficient, contact motion index and sliding work) at different compaction velocities, initial porosities and internal friction coefficients during ferrous powder compaction has been investigated by discrete element method. Results show that the small change in compaction velocity cannot influence the force chain characteristics and side wall friction behaviour. The different initial porosities and friction coefficients between particles can affect the force chain characteristics and the side wall friction behaviour. The force chain can be related to the side wall friction behaviour at different conditions, according to the corresponding characteristics of force chains and friction behaviour (before and after the axial strain reaches to 0.1). This study would expand the tribology of granular matter and is useful for understanding the internal and external mechanics during powder compaction.

Keywords Powder compaction · Granular matter · Discrete element method · Friction behavior · Force chain

1 Introduction

The metal powder compaction is an effective forming method to obtain compacts with a certain size and density under pressure [1]. This forming method has the advantages of low material loss, low cost and high efficiency. It also plays an important role in powder metallurgy and has been widely used in numerous fields, such as producing mechanical parts in engineering and composites in material science [2].

The friction during powder compaction, including internal and external friction, has effect on the densification process of compacts by limiting the rearrangement and displacement of powder [3]. The internal friction exists between powders, and the external friction behaviour occurs between powder and side walls of die; this condition is called side wall friction behaviour. Some works investigated the side wall friction behaviour during powder compaction. Chen et al. [4] analysed the friction behaviour of different metal powder mixtures by powder compaction experiments and found that large amount of lubricants can decrease the friction coefficient between side walls of die and mixtures. Zhou et al. [5] analyzed the friction coefficient between metal powder and side walls of die under lubricated and unlubricated conditions by finite element method (FEM). Staf and Larsson [6] carried out experiment and FEM simulation to investigate the role of side wall frictional model in analysing friction and friction coefficient during metal powder compaction. Combined with the previous works, the side wall friction behaviour is mostly analysed at macroscopic scale by numerical or experimental methods. Meanwhile, the friction coefficient and friction are commonly used in analysing side wall friction behaviour from macroscopic scale. However, the powder is a discontinuous system, and abundant powder particles are in contact with each other in this system. The side wall friction behaviour can be affected by particles, which are in contact with the side walls of die. The side wall friction behaviour should be further investigated at microscopic scale, and the microscopic friction parameters should be obtained to reveal detailed contact and motion

✉ Wei Zhang
zw1256@fjut.edu.cn

[1] School of Mechanical and Automotive Engineering, Fujian University of Technology, Fuzhou 350118, China

behaviour of particles. The microscopic friction analyze based on the granular matter is necessary.

The powder is a discrete system and belongs to granular matter, which contains particles with a diameter greater than 1 μm and liquid saturation less than 1 [7]. The discrete element method (DEM) can effectively investigate the granular matter [8], and the powder can be realised as a discontinuous medium based on DEM. The granular matter has multiscale mechanical behaviour, and mesoscopic force chain plays an important role in it. The force chain is a quasi linear mechanical structure with an adjacent contact force [9]. The force chains in powder can support external compaction load and provide the path for stress transmission. Some works have been conducted to investigate the force chains during powder compaction. Meng et al. [10] investigated the multiscale mechanical behaviour during powder compaction and qualitatively analysed the distribution of force chains indirectly via contact force statistics. Wang et al. [11] numerically analysed the compaction process of TiC-316L composite powders and discussed the formation and reorganisation of force chains qualitatively. We [12] also introduced quantitative parameters to describe the change of force chains during high velocity compaction of powder. However, the quantitative parameters of force chains are rather single. According to the above works, the change of force chains was mostly analysed qualitatively, and the quantitative parameters of force chains would describe the force chain information more directly. The detail quantitative research of force chains is also necessary.

Furthermore, although previous works have been carried out to investigate force chains or friction behaviour during powder compaction, the relation between force chains and side wall friction behaviour is uncertain. The side wall friction phenomenon is the external mechanical behaviour, and the evolution of force chains is the internal mechanical behaviour. An interaction between them is based on powder media. It's important to reveal the relation between internal mechanical behaviour and external friction behaviour during powder compaction from the perspective of microscopic granular matter. And internal and external powder compaction mechanism would be integrated based on it. It can be helpful for predicting internal mechanical behavior from external friction behavior or vice versa. More importantly, it would provide the basis for improving the densification during powder compaction based on external friction behaviour and internal mechanical mechanism.

Although the powder compaction could be investigated by 3D model, the 2D simulation also can be used to analyze the densification of powder in a cross section and to reveal the evolution of friction and mechanical characteristics [13, 14]. Moreover, to capture the force chains in 3D DEM model is an interesting topic. But the identification algorithm of force chains in 3D model is complex and difficult. Thus, most recent works about force chains have been done based on 2D planar DEM model [15, 16]. The 2D planar DEM model can provide a convenient way to capture the evolution of force chains. According to the above considerations, we use the 2D model to analyze the intrinsic mechanics and physics, including force chains and friction, during powder compaction. We would use the 3D model to compare the evolution of force chains and friction characteristics during powder compaction in 3D state to that in 2D state in the future.

The ferrous powder compaction model is established by DEM in Sect. 2 to investigate the side wall friction behaviour at particle scale and mesoscopic mechanics of powder system during powder compaction. The microscopic side wall friction characteristics and quantitative force chain characteristics are introduced in Sect. 3. The influence of compaction velocity, initial porosity and friction coefficient between particles on the side wall friction behaviour and force chain characteristics is analysed fully in Sect. 4. The relation between side wall friction behaviour and force chain is also discussed. This work would be helpful for expanding the granular matter friction mechanism and the mesoscopic mechanics of granular matter. And it can provide guidance for establishing the relation between internal and external granular matter behaviour. More importantly, it would provide the basis for improving the densification during powder compaction based on friction behaviour and internal mechanic mechanism.

2 Calculation model of powder compaction

2.1 DEM modelling process

The powder belongs to granular matter, and the process of powder compaction can be simulated by DEM. The powders can be realised as particles, and the motion of each particle is analysed by Newton's second law of motion in DEM [17], as follows:

$$\begin{cases} m_i \mathbf{g} + \sum \mathbf{f}_j = m_i \dfrac{d\mathbf{v}_i}{dt} \\ \sum \mathbf{f}_j \mathbf{r}_j = I_i \dfrac{d\boldsymbol{\omega}_i}{dt} \end{cases}, \tag{1}$$

where m_i and I_i are the mass and the moment of inertia of particle i, respectively; $\mathbf{f}_j$ and $\mathbf{r}_j$ are the contact force and the radius direction vector of j-th contact of particle i, respectively; $\boldsymbol{v}_i$ and $\boldsymbol{\omega}_i$ are the linear velocity and angular velocity of particle i, respectively; $\mathbf{g}$ is the gravitational acceleration, the value of such is 9.8 m/s^2 and with the same direction as the loading in this study.

Based on the motion law of powder, as shown in Eq. (1), the contact force is considered by contact model. The Hertz–Mindlin contact model is introduced to calculate the normal and tangential contact force between powders [17]. The damping condition is also considered to achieve the dissipation of energy [18]. The normal contact force is calculated by the following [17]:

$$\boldsymbol{F_n} = -K_n U_n \boldsymbol{n} - \eta_n \boldsymbol{G}_n, \tag{2}$$

where U_n is the normal overlap value between particles, η_n is the normal damping coefficient, $\boldsymbol{n}$ and $\boldsymbol{G}_n$ are the normal unit vector and the normal relative velocity between two particles, respectively. K_n is the normal contact stiffness obtained as follows [17]:

$$K_n = \left[\frac{2\tilde{G}\sqrt{2\tilde{R}}}{3(1-\tilde{\nu})}\right]\sqrt{U_n}, \tag{3}$$

where $\tilde{G}$,$\tilde{R}$ and $\tilde{\nu}$ are the equivalent shear modulus, radius and Poisson's ratio, respectively. They are calculated by the average shear modulus, radius and Poisson's ratio between two particles. In addition, if one particle is near the wall, the values of $\tilde{G}$,$\tilde{R}$ and $\tilde{\nu}$ are the shear modulus, radius and Poisson's ratio of this particle, respectively.

The tangential contact force is calculated by the following [17]:

$$\boldsymbol{F_t} = -K_t \boldsymbol{S} - \eta_t \boldsymbol{G}_t, \tag{4}$$

where $\boldsymbol{S}$ is the tangential displacement increment between two particles, η_t is the tangential damping coefficient, and $\boldsymbol{G}_t$ is the tangential relative velocity between two particles. K_t is the tangential contact stiffness obtained as follows:

$$K_t = \left[\frac{2\left(3\tilde{G}^2(1-\tilde{\nu})\tilde{R}\right)^{1/3}}{2-\tilde{\nu}}\right]\left|\boldsymbol{F}_n\right|^{1/3} \tag{5}$$

In addition, some other works used the stick–slip friction model to describe the effects of stick–slip behavior. Berry et al. [19] used the coulomb friction to model a stick and slip behaviour. The maximum tangential contact force is limited by the product of normal contact force and friction coefficient. Jasion et al. [20] introduced the stick–slip model based on the maximum tangential force which is the product of normal contact force and friction coefficient. Govender [21] pointed out that the tangential contact between particles is described by a stick–slip friction model where the tangential force is coupled to the normal force based on the Coulomb's law. Actually, the effects of stick–slip behavior have already been considered in our model according to the stick–slip friction model [19–21]. The tangential contact force is limited by the friction condition. If the tangential contact force is greater than the product of friction coefficient μ and the normal contact force, then the value of tangential contact force is set to the above product. It means that if the tangential contact force is greater than or equal to the $\mu\left|\boldsymbol{F_n}\right|$, the tangential contact force is calculated by $-\mu\boldsymbol{F_n}$. If the tangential contact force is less than $\mu\left|\boldsymbol{F_n}\right|$, the tangential contact force can be calculated by Eq. (4).

Although powder compaction can be investigated by 3 dimensions simulation, the 2 dimensions (2D) simulation can also be used to capture the displacement and rearrangement of powder and reveal the evolution of mechanical characteristics easily. The 2D DEM calculation model is shown in Fig. 1. The model consists of four die walls and has a width of 0.01 m and height of 0.015 m. The size of model is appropriate in powder compaction [22]. The left and right walls can be realised as side die walls, and the bottom wall can be realised as bottom punch. The loading wall is realised as the upper punch, and the compaction velocity is attributed to it along the negative direction of the *Y*-axis. The loading wall can move downward under the specified constant compaction velocity. The round ferrous powders are generated random in the die walls and then begin to settle down under gravity until they are relatively static [23]. A total of 3000 is used to improve computing efficiency. The material parameters of the powder is the same as the ferrous powder [14]. The density, Poisson's ratio and the elastic modulus of ferrous powder are 7800 kg/m^3, 0.25 and 209 GPa, respectively. The average diameter of the powder is 222 μm, and the range of particle size is 148 ~ 296 μm with the uniform distribution. The initial porosity of the system is 0.2. The porosity is calculated by the ratio of the difference between 1 and the area of powders to the area of model [17]. The

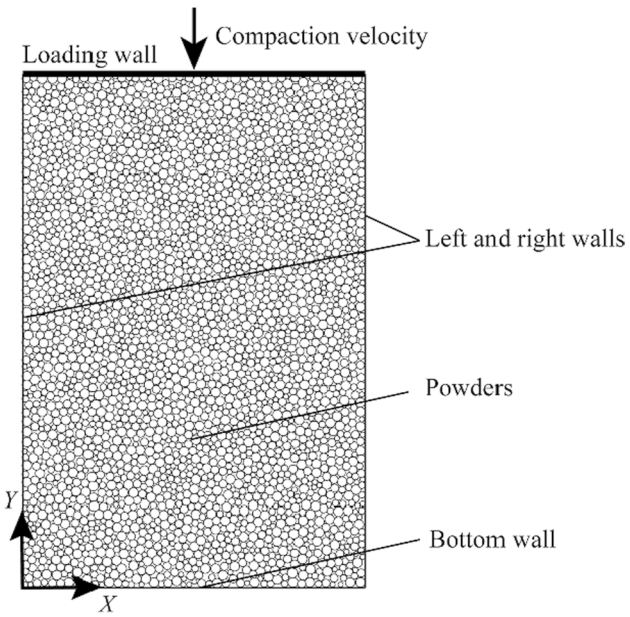

Fig. 1 DEM model of powder compaction

friction coefficient between powders and between powder and die walls is set to 0.25, which is selected based on Ref. [14]. The normal and tangential damping coefficient is 0.2, and it can achieve good energy dissipation [17]. Furthermore, we pay more attention to the effects of sliding friction between powders and between powder and die wall in this study. Some other works also ignore the effect of rolling friction and only consider the sliding friction coefficient between powders during simulation of powder compaction [10, 11, 24]. And there are also some reports about axial compression of granular materials only use the sliding friction coefficient between particles in the DEM model [25, 26]. Moreover, the rolling resistance model can be introduced by writing and coding an user-defined model (UDM) in C++and there are some papers pay more attention to it specifically [27, 28]. It is complex and difficult to combine with our current research. The role of rolling friction during powder compaction would be an interesting research and it would be investigated in the follow-up study.

During powder compaction, the loading wall moves downward with the compaction velocity of 0.2 m/s until the axial strain reaches 0.25. The axial strain is calculated by the ratio of the displacement of loading wall to the height of the model. The pressure can reach to approximately 600 MPa at axial strain of 0.25, and it is common in the ferrous powder compaction [14].

2.2 Fitting curve of compaction equation

The compaction behaviour of ferrous powder based on DEM model is analysed by the compaction curve to verify the reliability of the model. The compaction curve is fitted by the Athy–Shapiro–Konopicky equation, which is suitable for general metal powder and widely used in the medium- and high-pressure conditions [29, 30]. The Athy–Shapiro–Konopicky equation is given by the following:

$$\ln\left(\frac{1-\rho}{1-\rho_0}\right)=aP+b, \tag{6}$$

where P is the compaction pressure, and ρ and ρ_0 are the relative density and the initial relative density of powder, respectively. The relative density and the initial relative density of powder in DEM model can be calculated by the difference between 1 and the porosity and by the difference between 1 and the initial porosity. The calculation method of porosity is shown in Sect. 2.1. a and b in Eq. (6) are the fitting parameters. Suppose that $x=P$ and $y=\ln((1-\rho)/(1-\rho_0))$, the fitting curve is as shown in Fig. 2. The fitting equation is $y=-0.001086x-0.09188$, and the fitting correlation coefficient R^2 is 0.9898. The finding indicates that the DEM model satisfies the Athy–Shapiro–Konopicky equation, and the simulation model can describe the compaction behaviour of ferrous powder.

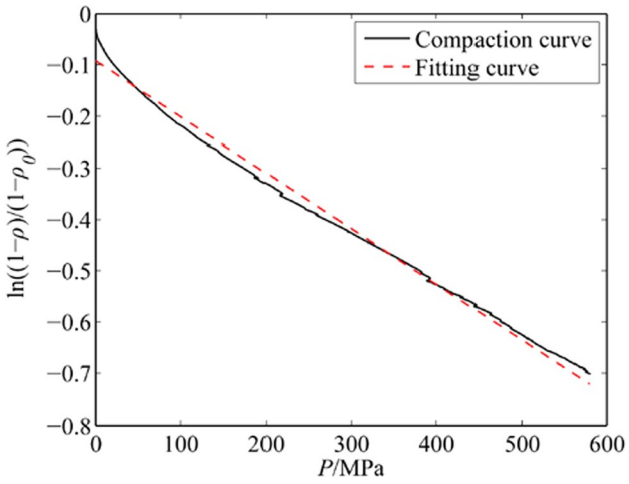

Fig. 2 Fitting curve of Athy–Shapiro–Konopicky equation (color online)

3 Quantitative analysis method

3.1 Analysis method of side wall friction behaviour

The nominal friction coefficient is introduced to describe the friction coefficient between powder and side walls. It can reflect the friction condition on the side wall. The nominal friction coefficient μ is calculated based on Amontons–Coulomb friction law [31], as follows:

$$\mu=\frac{\left|\frac{F_X^L}{F_Y^L}\right|+\left|\frac{F_X^R}{F_Y^R}\right|}{2}, \tag{7}$$

where F_X^L and F_Y^L are the normal and tangential force acting on the left side wall along the X-direction and Y-direction, respectively. F_X^R and F_Y^R are the normal and tangential force acting on the right side wall along the X-direction and Y-direction, respectively.

The contact motion index is also introduced to describe the contact condition of powders, which are in contact with the side walls [32]. The contact motion index can reflect the contact closest to the Coulomb failure criterion. If the contact motion index is 1, then all contacts satisfy the Coulomb failure criterion. The higher contact motion index indicates more difficulty for the powder to move. The contact motion index I_m is calculated by the following:

$$I_m = \frac{\sum_{i=1}^{s} \frac{f_i^t}{\mu_w f_i^n}}{s}, \tag{8}$$

where S is the number of contacts between the side wall and the powder, μ_w is the theoretical friction coefficient between the powder and the die walls, the value of which is 0.25. f_i^t and f_i^n are the tangential and normal contact forces of i-th contact on the side walls, respectively.

The sliding work can reflect the energy evolution of contacts on the side walls during powder compaction. The increment of sliding work ΔE_s during adjacent time steps is given by the following [17]:

$$\Delta E_s = \sum_{i=1}^{s} f_i^t \Delta U_i^s, \tag{9}$$

where ΔU_i^s is the increment of the displacement of i-th contact on the side walls during adjacent time steps.

3.2 Analysis method of force chain characteristics

The contact force judgment method [33] is used to obtain the information of force chains. The formation of force chains should satisfy three criteria, as follows: (1) strength criterion, where the contact force between particles of force chain should be greater than the mean value of contact force of powder; (2) length criterion, where the number of particles of one force chain should be more than three; (3) linearity criterion, where the sharp angle among three adjacent particles should be below the threshold to ensure the linearity of force chains. For example, the sharp angle amongst particles 1, 2 and 3 is the difference of 180° and β_1, as shown in Fig. 3. The threshold is calculated by the ratio of the 180° and the average coordination number, which is the average contact number of every particle. If some neighbouring particles satisfy the above three criteria, they would form one force chain. The force chains are extracted until all the particles of the system are considered. The detailed extraction method of the force chains of the powder is in accordance with Ref. [33] and our previous work [12].

Furthermore, the quantitative parameters are introduced to describe the force chain characteristics, including number, length, direction coefficient, and buckling degree, based on the information of force chains.

The length of force chain is calculated by the sum of distance between every adjacent particle in the force chain, as follows:

$$l = \sum_{i=1}^{n-1} d_{i,i+1}, \tag{10}$$

where n is the number of particles in this force chain, and $d_{i,i+1}$ is the distance between i-th particle and $(i+1)$-th particle. For example, the length of force chain in Fig. 3 is the sum of $d_{1,2}$, $d_{2,3}$ and $d_{3,4}$.

The direction coefficient of force chain can describe the extension direction of force chain [34]. The direction coefficient of force chain is calculated by the following:

$$R_d = \frac{\sum_{i=1}^{n-1} \frac{|\delta_{i,i+1}|}{90^\circ}}{n-1}, \tag{11}$$

where $\delta_{i,i+1}$ is the included sharp angle between the direction of i-th contact force of force chain and the direction of Y-axis. The direction of i-th contact force is along that of $d_{i,i+1}$. For example, the direction of f_1 (first contact force) is along the direction of $d_{1,2}$, as shown in Fig. 3. Lower R_d indicates that the force chain inclines to the Y-axis more remarkably.

The buckling degree of force chain can describe the linearity of force chain. It is calculated by the following:

$$R_b = \frac{\sum_{i=1}^{n-2} \frac{180^o - \beta_i}{180^o}}{l}, \tag{12}$$

where β_i is the angle between $d_{i,i+1}$ and $d_{i+1,i+2}$. For example, β_1 is the angle between $d_{1,2}$ and $d_{2,3}$ in Fig. 3. The higher R_b indicates worse linearity degree of force chain.

The length, direction coefficient and buckling degree of all force chains of the powder system are analysed, and their average value is obtained to represent the force chain characteristics of the system during powder compaction.

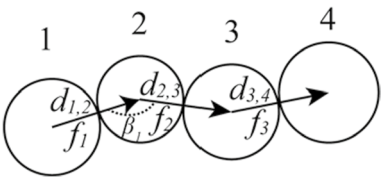

Fig. 3 Diagram of force chain quantitative characteristics

4 Results and discussions

4.1 Influence of compaction velocity

The compaction velocity is the key factor for powder densification. The influence of compaction velocity ($v = 0.1$, 0.2, 0.3, 0.4 and 0.5 m/s) on side wall friction behaviour is obtained, as shown in Fig. 4.

With the increase in axial strain, the nominal friction coefficient and the contact motion index increase initially and then maintain fluctuation. The nominal friction

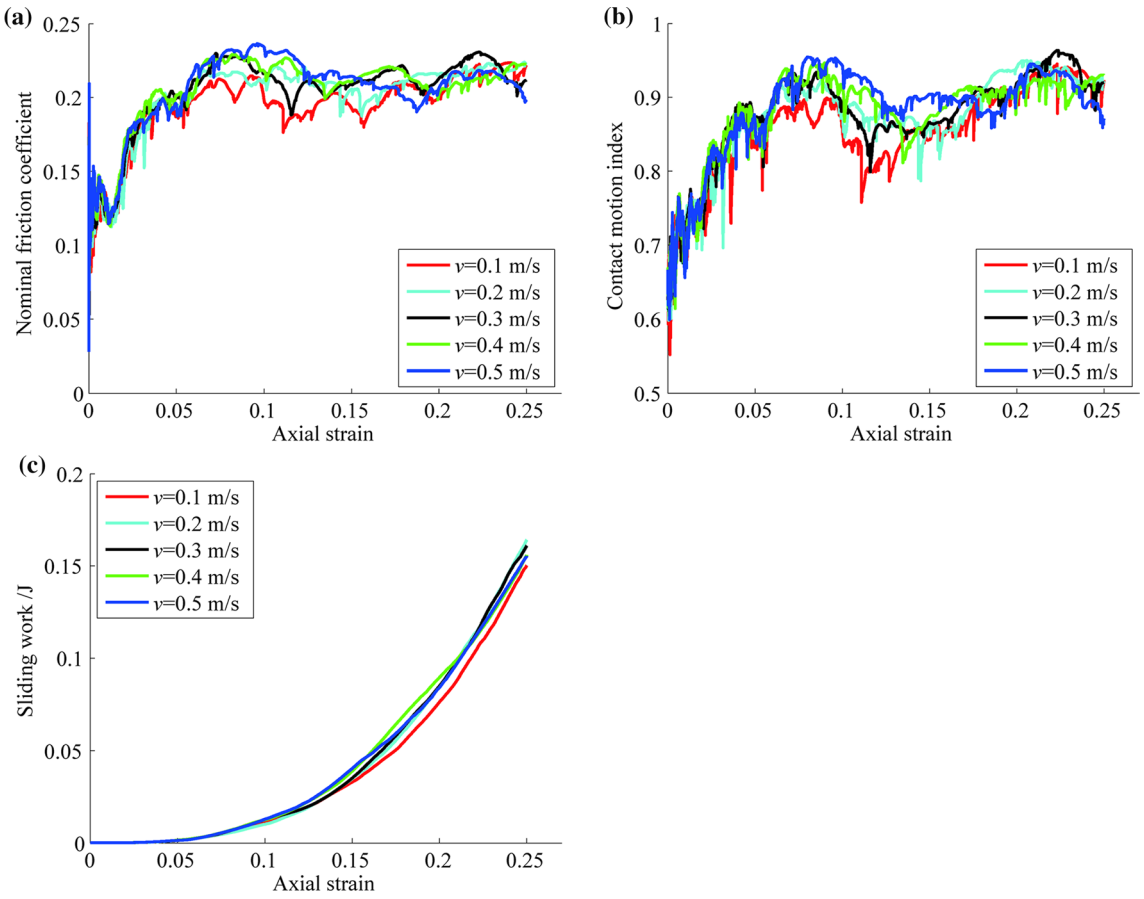

Fig. 4 Evolution of side wall friction behaviour at different velocities: **a** nominal friction coefficient, **b** contact motion index and **c** sliding work. (color online)

coefficient increases when the axial strain is less than 0.1 and remain constant (approximately 0.22) when the axial strain is greater than 0.1. According to Ref. [4], the friction coefficient also increases initially and then remains constant. The contact motion index increases initially when the axial strain is less than 0.1, then has a slight reduction. Finally, the contact motion index fluctuates gradually. With the increase in axial strain, the sliding work continues to increase. The growth rate is relatively low when the axial strain is less than 0.1 and is relatively high when the axial strain is greater than 0.1. The evolution of friction behaviour is related to the densification of powder. The powder begins to move and rearrange when the axial strain is low. The friction coefficient and contact motion index increase, and the sliding work increases slowly in this stage. Then, the structure of the powder inclines to be stable gradually, and the friction coefficient and contact motion index slightly change. Meanwhile, the sliding work has rapid growth in this stage based on the relatively more contact between powder and side walls.

The influence of compaction velocity on the nominal friction coefficient, the contact motion index and the sliding work is small (Fig. 4). With the increase in compaction velocity, the friction coefficient and the contact motion index increase slightly. The relatively high compaction velocity rearranges the powder more dramatically, and the friction resistance is slightly high between power and side walls when the change of compaction velocity is small.

The evolution of force chain characteristics and the influence of compaction velocity are shown in Fig. 5.

With the increase in axial strain, the number of force chains increases gradually, and the length of force chains decreases gradually. This finding indicates that the force chains change from long force chains to short force chains based on the break and reorganisation of force chains. The newly generated force chains have better linearity; thus, the buckling degree decreases with the increase in axial strain. With the increase in axial strain, the force chains incline to the compaction load direction and play the role as load bearing. Thus, the direction coefficient of force chains decreases and the anisotropy of all force chains enhance initially. Meng et al. [10] also found the change in anisotropy of contact force during powder compaction. Then, the direction coefficient of force chains remains stable, and the anisotropy does not change remarkably.

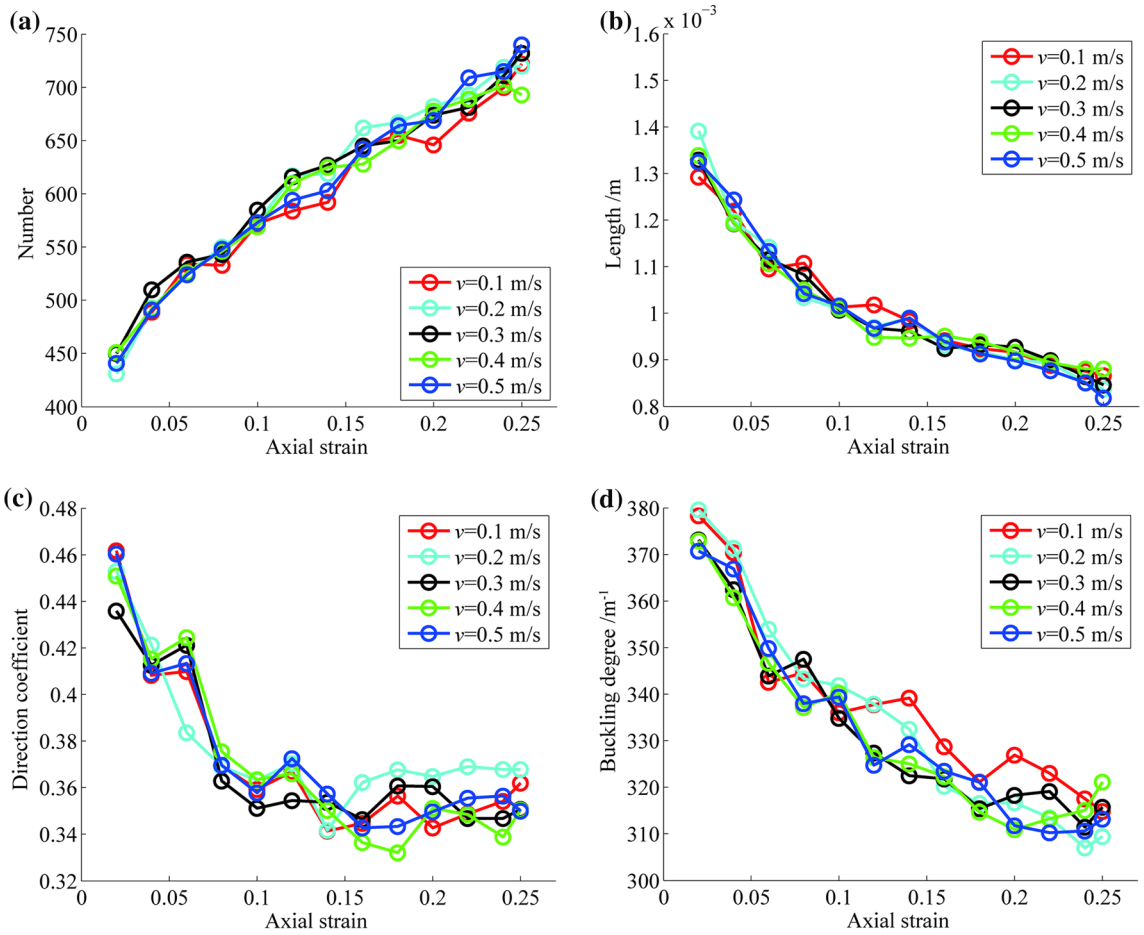

Fig. 5 Evolution of force chain characteristics at different velocities: **a** number, **b** length, **c** direction coefficient and **d** buckling degree. (color online)

Interestingly, the change of force chain characteristics corresponds to the change of side wall friction behaviour during powder compaction at different velocities (Figs. 4 and 5). With the increase in axial strain, the length and buckling degree of force chains decrease rapidly when the axial strain is less than 0.1 and decrease slowly when the axial strain is greater than 0.1. The direction coefficient of force chains decreases rapidly when the axial strain is less than 0.1 and remains approximately 0.35 when the axial strain is greater than 0.1. The number of force chains increases with the increase in axial strain, and the growth rate with the axial strain is less than 0.1, which is slightly higher than that when the axial strain is greater than 0.1. Meanwhile, the evolution of side wall friction behaviour has a significant difference before and after axial strain reaches to 0.1 (Fig. 4).

With the increase in the friction coefficient, the contact motion index and the sliding work, the friction resistance of powder enhances. The flow ability of powder becomes worse. Then, the friction resistance of powder remains relatively stable, as well as the powder structure when the axial strain is greater than 0.1. Thus, the changes in force chain characteristics are small when the axial strain is greater than 0.1 (Fig. 5). The side wall friction can affect the motion of powder and influences the force chains in the powder system. The evolution of force chain can also cause friction coefficient and the contact motion index to increase initially and then remain stable. When the axial strain is greater than 0.1, the short force chains with better linearity can lead to uniform load distribution in the powder system, and the structure of the powder becomes stable. Thus, the powder near the side walls is difficult to change its motion condition, and the friction coefficient and contact motion index become steady when the axial strain is greater than 0.1 (Fig. 4).

Furthermore, the compaction velocity may not have remarkable influence on the force chain characteristics and have slight influence on the side wall friction behaviour when the change in compaction velocity is small. In summary, the evolution of force chain characteristics can be related to the side wall friction behaviour during powder compaction at different compaction velocities.

4.2 Influence of initial porosity

The dense or loose initial structure of powder may affect the friction behaviour during powder compaction. The initial porosity can describe the density of powder structure. High initial porosity indicates that powder is loose. The low initial porosity indicates that the powder is dense. The influence of initial porosity ($\gamma = 0.24, 0.22, 0.2, 0.18, 0.16$) on the side wall friction behaviour is obtained, as shown in Fig. 6.

With the increase in axial strain, the nominal friction coefficient and contact motion index increase initially, and then maintain a relatively steady state at different initial porosities. The sliding work increases with the increase in axial strain. The initial porosity has a remarkable influence on the side wall friction behaviour. The high initial porosity can cause the powder structure to become loose initially, and it can make the evolution of nominal friction coefficient and contact motion index to be dramatic when the axial strain is less than 0.1. The increase in nominal friction coefficient and contact motion index has the most remarkable fluctuations when the initial porosity is 0.24, as shown in Fig. 6(a) and (b). The loose powder structure can lead to the substantial powder displacement and rearrangement; thus, the contact condition between the powder and side walls changes frequently. In addition, the evolution of nominal friction coefficient and contact motion index is dramatic and frequent at high initial porosity when the axial strain is less than 0.1. This finding indicates that the high initial porosity of powder may have disadvantages for powder densification according to the frequent changes in friction condition. When the axial strain is greater than 0.1, the powder structure becomes close, and the evolution of friction coefficient and contact motion index has a slight difference at different initial porosities. The sliding work increases slowly when the axial strain is less than 0.1 and then increases rapidly, as shown in Fig. 6(c). The high porosity also corresponds to the small change in sliding work. It can be attributed to the loose powder structure with small number of powders which are in contact with the side walls. And the relative sliding work increment of powders is small. Solimanjad et al. [35] also found that the initial relative density can affect the friction

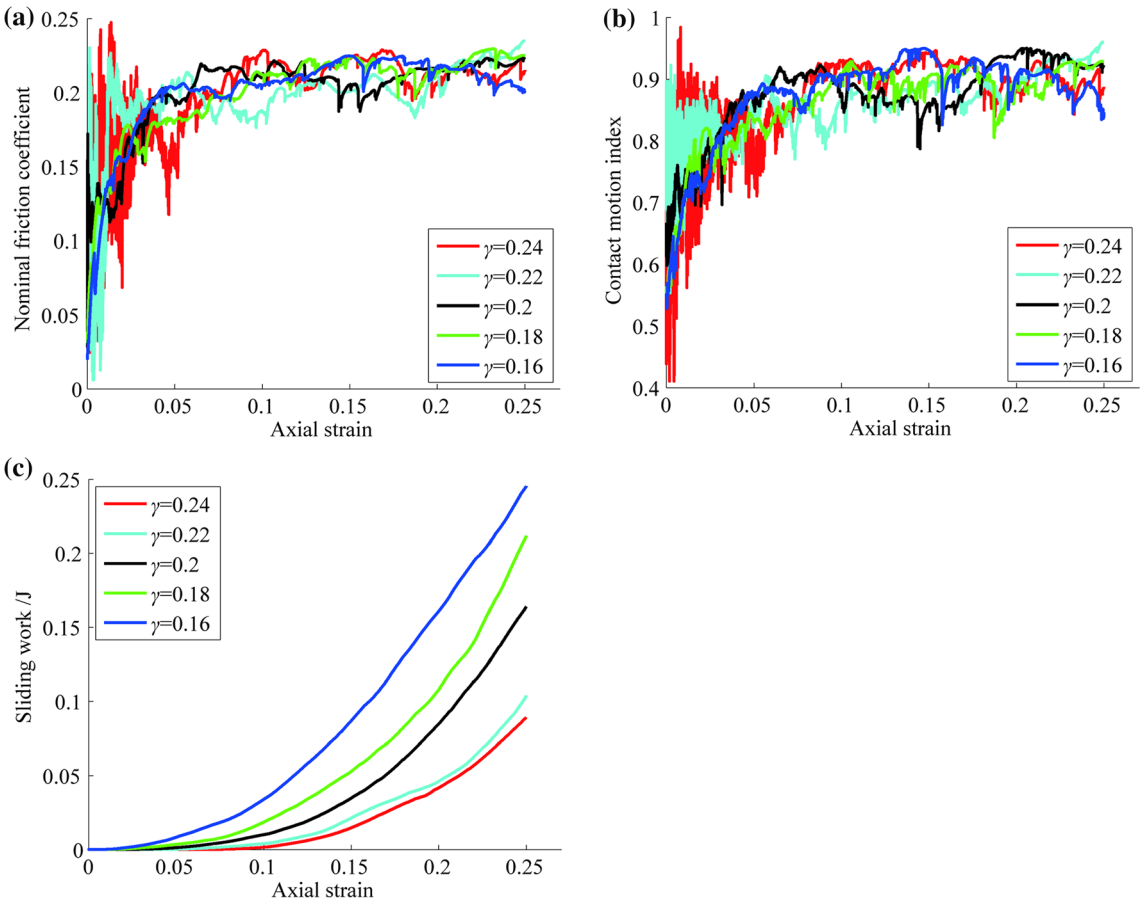

Fig. 6 Evolution of side wall friction behaviour at different initial porosities: **a** nominal friction coefficient, **b** contact motion index and **c** sliding work. (color online)

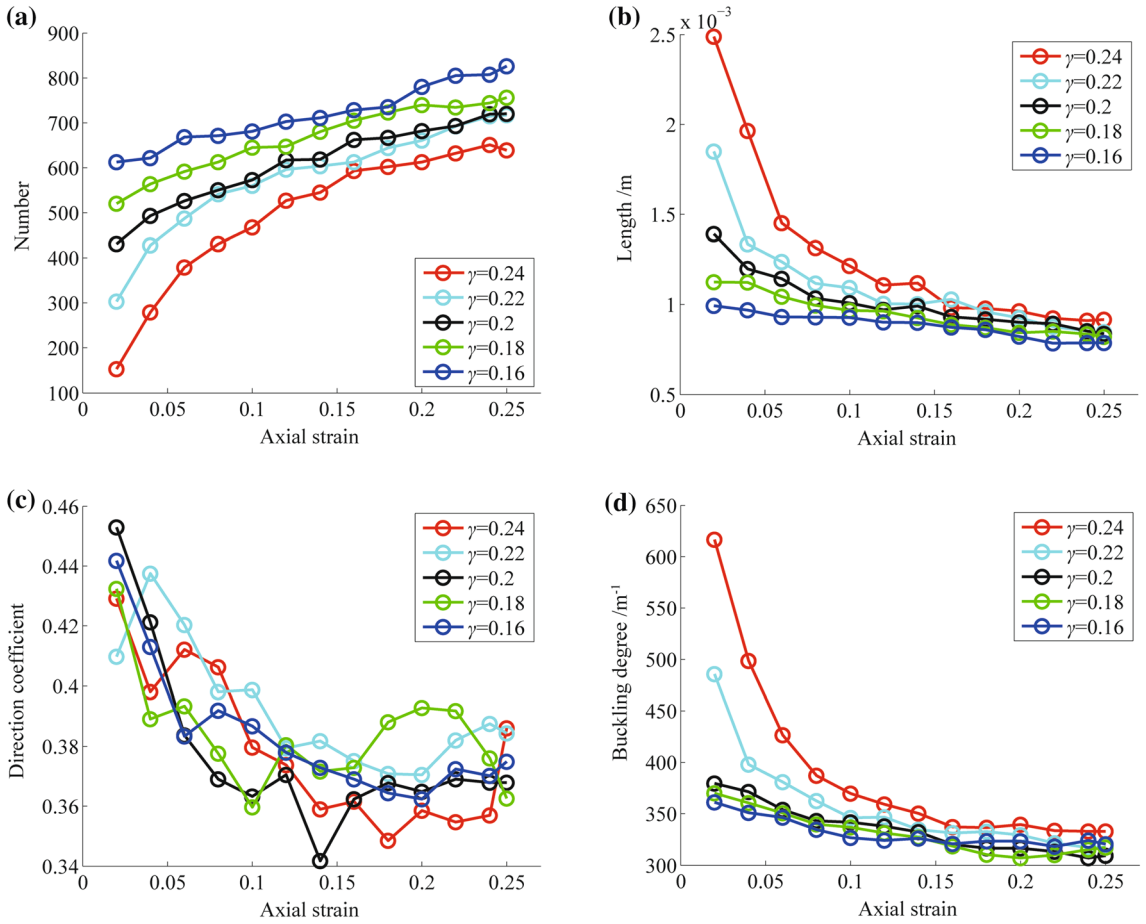

Fig. 7 Evolution of force chain characteristics at different initial porosities: **a** number, **b** length, **c** direction coefficient and **d** buckling degree. (color online)

behaviour at macroscopic scale by ferrous powder compaction experiments.

The influence of initial porosity on the evolution of force chain characteristics is shown in Fig. 7.

With the increase in axial strain, the number of force chains increases rapidly initially and then increases slowly gradually. The length, direction coefficient and buckling degree of force chains decrease when the axial strain is less than 0.1, and then incline to steady gradually when the axial strain is greater than 0.1. The increase in force chain number and the decrease in force chain length and buckling degree are significant at high initial porosity. The initial porosity may not influence the force chain' direction coefficient. The powder can achieve close contact structure gradually during powder compaction, and the initial powder structure is loose at high initial porosity. The displacement and rearrangement of powder are dramatic, and the probability of forming force chains undergoes great change when the initial porosity is high. Thus, the increase in force chain number is remarkable. The evolution of powder structure and the flow of powder are dramatic, and the number of newly generated force chain is great during powder compaction, according to the increase in force chain number at high initial porosity. The existing force chains are broken down under compaction load and can form many new short force chains with better linearity with the increase in axial strain at high initial porosity. Thus, the change in force chain length and buckling degree is significant at high initial porosity.

Figures 6 and 7 show that the evolution of side wall friction behaviour is related to the evolution of force chain characteristics at different initial porosities. The evolution of force chain characteristics is relatively remarkable when the axial strain is less than 0.1. And the nominal friction coefficient and contact motion index show fluctuating increase when the axial strain is less than 0.1. Moreover, the change in number, length and buckling degree of force chains is great at high initial porosity, and the fluctuation of friction coefficient and contact motion index is dramatic at high initial porosity. On the one hand, the evolution of force chain characteristics can affect the stress distribution within the powder system under external compaction load and change the powder structure rapidly at high initial porosity when the

axial strain is less than 0.1. It can further cause significant fluctuation of side wall friction condition when the axial strain is less than 0.1. On the other hand, the increase in side wall friction coefficient and contact motion index with fluctuations can also change the powder structure frequently, and then form relatively stable structure at high initial porosity. This condition can be beneficial for the substantial change in the number, length and buckling degree of force chains in powder system. Thus, the evolution of force chain characteristics and side wall friction behaviour at different initial porosities has a relationship during powder compaction.

4.3 Influence of friction coefficient between particles

The friction during powder compaction includes two parts, namely, external friction and internal friction. The friction coefficient between particles can describe the internal friction obstruction between powders and is related to the external friction, which reflects the side wall friction condition. The influence of friction coefficient between particles (μ_p = 0.05, 0.15, 0.25, 0.35, 0.45) on side wall friction behaviour is obtained, as shown in Fig. 8.

With the increase in axial strain, the nominal friction coefficient and contact motion index increase initially and then remain relatively stable in general at different friction coefficients between particles. The increases in nominal friction coefficient and contact motion index are remarkable when the axial strain is less than 0.1, and they exhibit fluctuations but remain relatively steady when the axial strain is greater than 0.1. Furthermore, the sliding work increases gradually with the increase in axial strain, and its growth rate becomes greater gradually when the axial strain is greater than 0.1. When the friction coefficients between particles are 0.05, 0.15, 0.25, 0.35 and 0.45, the nominal friction coefficients at relatively stable stage incline to 0.04, 0.14, 0.22, 0.23 and 0.24, respectively, as shown in Fig. 8(a). This finding indicates that the internal friction coefficient of powder can affect the external nominal friction coefficient of powder. The internal and external friction coefficients incline to the same value when the powder in contact with side walls is partial sliding,

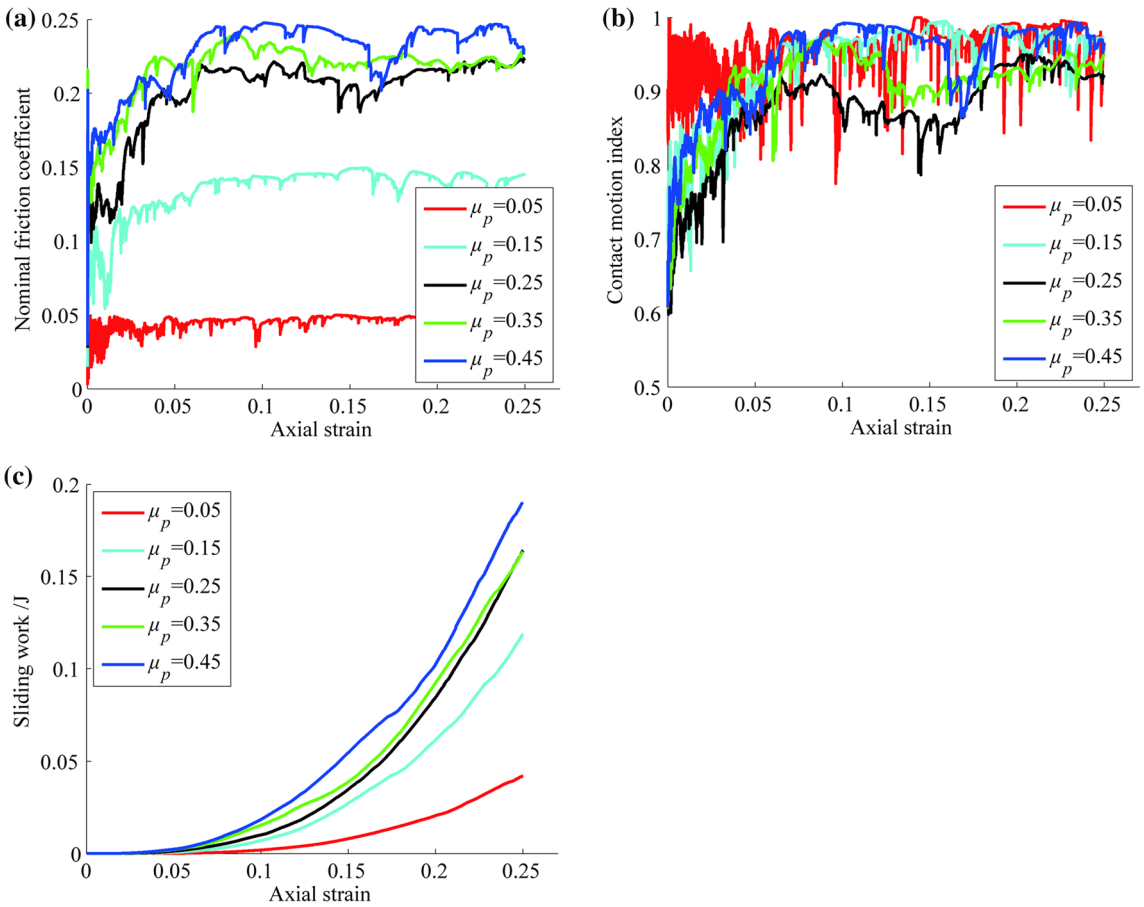

Fig. 8 Evolution of side wall friction behaviour at different friction coefficients between particles: **a** nominal friction coefficient, **b** contact motion index and **c** sliding work. (color online)

and the external friction coefficient slightly changes when the internal friction coefficient is sufficiently high. Thus, the internal and external lubrication of powder should be both considered to improve densification during powder compaction [36]. The fluctuation of contact motion index is dramatic when the friction coefficient between particles is small, as shown in Fig. 8(b). This finding can be attributed to that the small friction coefficient between particles is helpful for motion of powder and causes it to flow more easily. In addition, the contact condition can change more frequently. Thus, the fluctuation of contact motion index is dramatic at low friction coefficient between particles. With the increase in friction coefficients between particles, the relative motion between powder and side walls becomes difficult and the friction become greater. Thus, the increase in sliding work, which is caused by friction, becomes more remarkable, as shown in Fig. 8(c).

The influence of friction coefficient between particles on the evolution of force chain characteristics is obtained, as shown in Fig. 9.

The number of force chains increases and the length and buckling degree of force chains decrease gradually at different friction coefficients between particles with the increase in axial strain. With the increase in axial strain, the direction coefficient of force chains decreases at different friction coefficients between particles, except when the friction coefficient between particles is 0.45. This finding indicates that the high friction coefficient between particles would not effective for force chains to adjust direction. The low-friction coefficient between particles corresponds to the significant increment of number of force chains, as shown in Fig. 9(a). The finding can be attributed to the weak resistance of relative motion between powders, thereby causing the powder to rearrange and form force chains more easily. The low-friction coefficient between particles also corresponds to the short length, low buckling degree and high direction coefficient of force chains, as shown in Fig. 9(b), (c) and (d). When the friction coefficient between particles is low, the flow ability of the powder is good, and the powder structure is easily

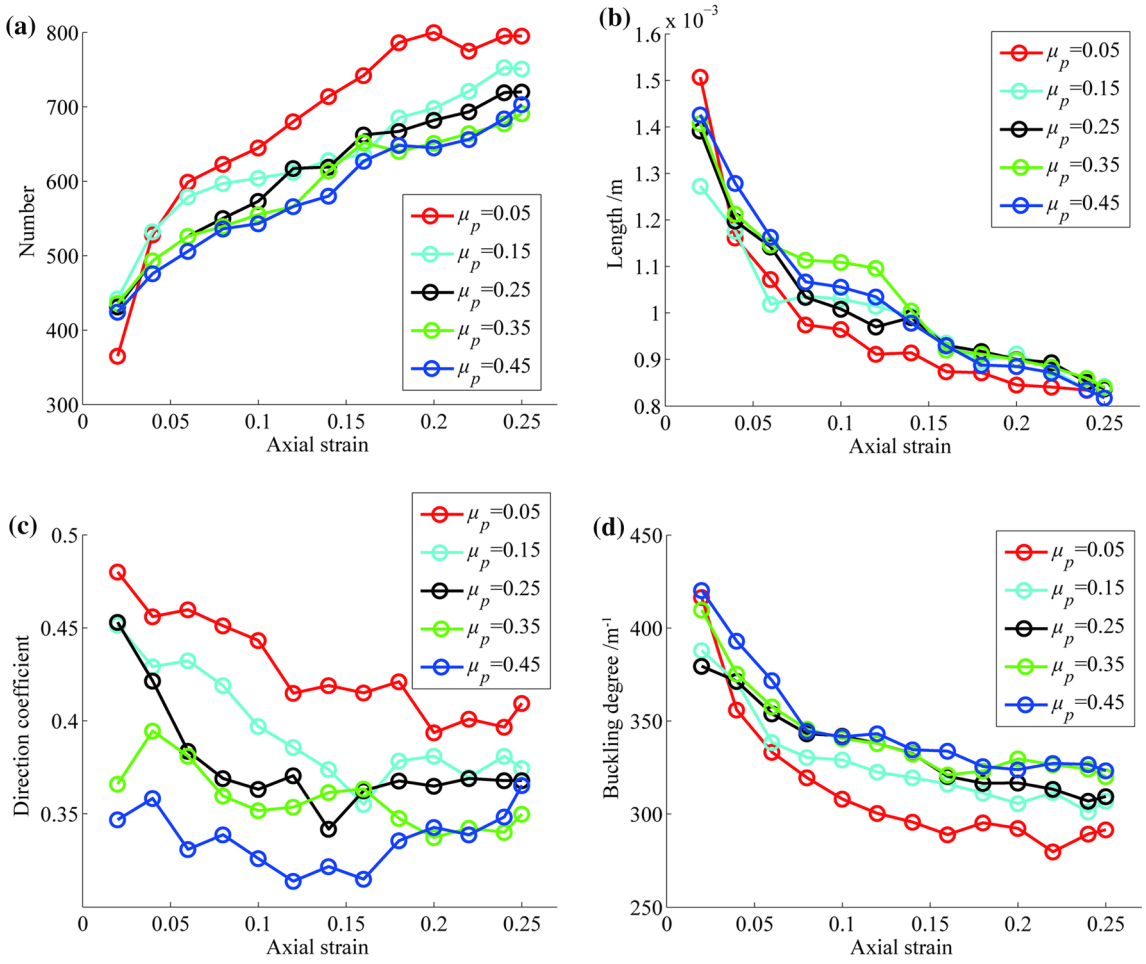

Fig. 9 Evolution of force chain characteristics at different friction coefficients between particles: **a** number, **b** length, **c** direction coefficient and **d** buckling degree. (color online)

adjusted. The short-force chains with good linearity are formed more easily, and the force chains have a relatively low probability to incline to the direction of external load because powders can move and rearrange easily.

The relationship between force chain characteristics and side wall friction behaviour at different friction coefficients between particles can be found based on Figs. 8 and 9. The nominal friction coefficient and contact motion index increase when the axial strain is less than 0.1. Meanwhile, the buckling degree and length of force chains decrease when the axial strain is less than 0.1. The nominal friction coefficient and contact motion index fluctuate and remain relatively stable when the axial strain is greater than 0.1. In addition, the buckling degree and length of force chains have small reduction when the axial strain is greater than 0.1. The evolution of side wall friction behaviour indicates that the relative motion between powder and side walls becomes difficult gradually when the axial strain is less than 0.1, and the powder structure becomes stable based on the large side wall friction resistance when the axial strain is greater than 0.1. This condition would enable the force chains to adjust rapidly and then remain relatively stable. The new short force chains with low buckling degree would appear under the external compaction load. Thus, the buckling degree and length of force chains decrease initially and then slightly decrease. Meanwhile, the new short force chains with low buckling degree in the system can also support the powder structure and stabilise it gradually when the axial strain is greater than 0.1. Thus, the change in side wall friction behaviour decreases.

Moreover, the influence of friction coefficient between particles on force chain characteristics corresponds to that on side wall friction behaviour. The low-friction coefficient between particles corresponds to the large number, short length, good linearity and weak anisotropy of force chains according to Fig. 9. The low-friction coefficient between particles corresponds to the low nominal friction coefficient, dramatic fluctuation of contact motion index and small sliding work according to Fig. 8. The small friction resistance between powder and side walls is obtained from the low-friction coefficient between particles; thus, the powder is rearranged and adjusted more easily. Thus, the powder becomes relatively dense, and the close structure of the powder would cause the force chains to have short length, good linearity and weak anisotropy at the low-friction coefficients between particles. In summary, some relationships are found between the evolution of force chain characteristics and side wall friction behaviour during powder compaction at different friction coefficients between particles.

5 Conclusions

The process of ferrous powder compaction is simulated using DEM based on granular matter mechanicas. The evolution of the side wall friction behaviour and force chain quantitative characteristics are investigated. The influence of compaction velocity, initial porosity and friction coefficient between particles on side wall friction behaviour and force chain characteristics are discussed. Furthermore, the relation between force chains and friction behaviour is studied. Some new phenomena, including dynamic evolution of microscopic friction parameters and influence of different factors on friction behavior, as well as evolution of force chain quantitative parameters and the dependences of force chain characteristics on different factors, etc., are found. The main conclusion can be drawn as follows:

(1) During powder compaction process, the nominal friction coefficient and contact motion index increase initially then continuously fluctuates. In addition, the sliding work increases gradually at different compaction velocities ($v = 0.1$, 0.2, 0.3, 0.4 and 0.5 m/s). The number of force chains increases gradually, and the length and buckling degree of force chains decrease gradually. The direction coefficient of force chains decreases initially and then continuously fluctuates. The evolution of force chain characteristics and side wall friction behaviour have remarkable differences before and after the axial strain reaches 0.1 at different compaction velocities. Moreover, the compaction velocity slightly influence the force chain characteristics and side wall friction behaviour when the change in compaction velocity is small.

(2) During powder compaction process, the nominal friction coefficient and contact motion index increase initially and then continuously fluctuates, and the sliding work increases gradually at different initial porosities ($\gamma = 0.24$, 0.22, 0.2, 0.18 and 0.16). The high initial porosity causes the increase in nominal friction coefficient and contact motion index to fluctuate dramatically and decreases the increase in sliding work. At different initial porosities, the number of force chains increases gradually and the length or buckling degree of force chains decreases gradually. The direction coefficient of force chains decreases initially and then continues to fluctuate. The high initial porosity would be related to the long length, small number and high buckling degree of force chains.

(3) During the powder compaction process, the nominal friction coefficients increase initially and then incline to the friction coefficients between particles ($\mu_p = 0.05$, 0.15, 0.25), and the nominal friction coefficients incline

to 0.23 and 0.24 when μ_p is 0.35 and 0.45. The low-friction coefficient between particles cause the dramatic fluctuation of contact motion index. The sliding work increases gradually with the increase in axial strain and the increase of sliding work is small at low-friction coefficient between particles. At different friction coefficients between particles, the number of force chains increases gradually, and the length or buckling degree of force chains decreases gradually with the increase in axial strain. The direction coefficient of force chains decreases initially and then remains stable, except when the friction coefficient between particles is 0.45. The low-friction coefficient between particles corresponds to the large number, short length, low buckling degree and high direction coefficient of force chains.

(4) The evolution of force chain characteristics and side wall friction behaviour has a relationship at different compaction velocities, initial porosities and friction coefficients between particles, according to the corresponding quantitative characteristics of force chains and side wall friction behaviour (before and after the axial strain reaches to 0.1), as well as the different influences of compaction velocity, initial porosity and friction coefficient between particles. The corresponding evolution between force chain characteristics and side wall friction behaviour is observed.

Acknowledgements This work was supported by the Natural Science Foundation of Fujian Province (Grants No. 2020J01869 and 2020J01874) and the Initial Scientific Research Fund in Fujian University of Technology (Grant No. GY-Z19123). The first author specifically thanks his lover, Dr. Rongxin Chen.

Declarations

Conflict of interest The authors have no competing interests to declare that are relevant to the content of this article.

References

1. Staf, H., Kis, Z., Szentmiklósi, L., et al.: Determining the density distribution in cemented carbide powder compacts using 3D neutron imaging. Powder. Technol. **354**, 584–590 (2019). https://doi.org/10.1016/j.powtec.2019.06.033
2. Nicewicz, P., Sano, T., Hogan, J.D.: Confined uniaxial compression of granular stainless steel 316. Powder. Technol. **353**, 489–497 (2019). https://doi.org/10.1016/j.powtec.2019.05.041
3. Shin, D.S., Lee, C.H., Kim, S.H., et al.: Analysis of cold compaction for Fe-C, Fe-C-Cu powder design based on constitutive relation and artificial neural networks. Powder. Technol. **353**, 330–344 (2019). https://doi.org/10.1016/j.powtec.2019.05.042
4. Chen, W.C., Wang, J.H., Wang, S.P., et al.: On the processing properties and friction behaviours during compaction of powder mixtures. Mater. Sci. Tech-Lond. **36**, 1057–1064 (2020). https://doi.org/10.1080/02670836.2020.1747779
5. Zhou, M.C., Huang, S.Y., Lei, Y., et al.: Investigation on compaction behaviors of Ag35Cu32Zn33 mixed metal powders under cold die compaction. J. Adv. Mech. Des. Syst. **12**, JAMDSM0037 (2018). https://doi.org/10.1299/jamdsm.2018jamdsm0037
6. Staf, H., Larsson, P.L.: Evaluation of an advanced powder-die frictional model. Powder. Technol. **363**, 569–574 (2020). https://doi.org/10.1016/j.powtec.2020.01.048
7. de Gennes, P.G.: Granular matter: a tentative view. Rev. Mod. Phys. **71**, S374-382 (1999). https://doi.org/10.1103/RevModPhys.71.S374
8. Zuo, P.C., Yu, H., Liu, J.L., et al.: Tensile and shearing behaviors of the particle raft. Acta. Mech. Sin. **37**, 907–912 (2021). https://doi.org/10.1007/s10409-021-01081-3
9. Zhang, X.J., Sun, W., Wang, W., et al.: Experimental investigation of granular friction behaviors during reciprocating sliding. Friction (2021). https://doi.org/10.1007/s40544-021-0488-2
10. Meng, F.J., Liu, K., Qin, T.: Numerical analysis of multi-scale mechanical theory of densified powder compaction. J. Braz. Soc. Mech. Sci. **40**, 430 (2018). https://doi.org/10.1007/s40430-018-1337-8
11. Wang, D.F., An, X.Z., Han, P., et al.: Particulate scale numerical investigation on the compaction of TiC-316L composite powders. Math. Probl. Eng. **2020**, 5468076 (2020). https://doi.org/10.1155/2020/5468076
12. Zhang, W., Zhou, J., Zhang, X.J., et al.: Quantitative investigation into the relation between force chains and stress transmission during high-velocity compaction of powder. J. Korean. Phys. Soc. **74**, 660–673 (2019). https://doi.org/10.3938/jkps.74.660
13. Olsson, E., Larsson, P.L.: A numerical analysis of cold powder compaction based on micromechanical experiments. Powder Technol. **243**, 71–78 (2013). https://doi.org/10.1016/j.powtec.2013.03.040
14. Lei, Y., Yan, S., Huang, S., et al.: Experimental and numerical investigation of densification behaviors during powder compaction. J. Adv. Mech. Des. Syst. Manuf. **12**, JAMDSM0022 (2018). https://doi.org/10.1299/jamdsm.2018jamdsm0022
15. Xu, R., Liu, E., Jiang, X., et al.: Analysis on evolution of mesostructure of cohesionless soil ground upon loading. Powder Technol. **368**, 1–17 (2020). https://doi.org/10.1016/j.powtec.2020.04.048
16. Liu, J., Wautier, A., Bonelli, S., et al.: Macroscopic softening in granular materials from a mesoscale perspective. Int. J. Solids Struct. **193**, 222–238 (2020). https://doi.org/10.1016/j.ijsolstr.2020.02.022
17. Itasca Consulting Group Inc: PFC2D (Particle Flow Code in 2 Dimensions). Itasca Consulting Inc, Minneapolis (1999)
18. Caserta, A.J., Navarro, H.A., Cabezas-Gómez, L.: Damping coefficient and contact duration relations for continuous nonlinear spring-dashpot contact model in DEM. Powder. Technol. **302**, 462–479 (2016). https://doi.org/10.1016/j.powtec.2016.07.032
19. Berry, N., Zhang, Y., Haeri, S.: Lees-Edwards boundary conditions for the multi-sphere discrete element method. Powder Technol. **389**, 292–308 (2021). https://doi.org/10.1016/j.powtec.2021.05.025
20. Jasion, G.T., Shrimpton, J.S., Li, Z., et al.: On the bridging mechanism in vibration controlled dispensing of pharmaceutical powders from a micro hopper. Powder Technol. **249**, 24–37 (2013). https://doi.org/10.1016/j.powtec.2013.07.027
21. Govender, N.: Study on the effect of grain morphology on shear strength in granular materials via GPU based discrete element method simulations. Powder Technol. **387**, 336–347 (2021). https://doi.org/10.1016/j.powtec.2021.04.038
22. Mehr, F.R., Salavati, M., Morgenthal, A., et al.: Computational analysis and experimental calibration of cold isostatic compaction of Mg-SiC nanocomposite powders. Mater. Today. Commun. **27**, 102321 (2021). https://doi.org/10.1016/j.mtcomm.2021.102321

23. Jiang, M.J., Konrad, J.M., Leroueil, S.: An efficient technique for generating homogeneous specimens for DEM studies. Comput. Geotech. **30**, 579–597 (2003). https://doi.org/10.1016/S0266-352X(03)00064-8
24. Garner, S., Strong, J., Zavaliangos, A.: Study of the die compaction of powders to high relative densities using the discrete element method. Powder Technol. **330**, 357–370 (2018). https://doi.org/10.1016/j.powtec.2018.02.015
25. Meng, F.J., Liu, K.: Mechanical study on the effect of granular friction in a granular system under biaxial compression. J. Korean Phys. Soc. **72**, 1179–1187 (2018). https://doi.org/10.3938/jkps.72.1179
26. Nie, Z., Qi, Q., Wang, X., et al.: DEM investigation of strain behaviour and force chain evolution of gravel–sand mixtures subjected to cyclic loading. Particuology **68**, 13–28 (2022). https://doi.org/10.1016/J.PARTIC.2021.10.006
27. Liu, Y., Liu, H., Mao, H.: The influence of rolling resistance on the stress-dilatancy and fabric anisotropy of granular materials. Granul. Matter. **20**, 12 (2018). https://doi.org/10.1007/s10035-017-0780-z
28. Mohamed, A., Gutierrez, M.: Comprehensive study of the effects of rolling resistance on the stress–strain and strain localization behavior of granular materials. Granul. Matter. **12**, 527–541 (2010). https://doi.org/10.1007/s10035-010-0211-x
29. Kawakita, K., Lüdde, K.H.: Some considerations on powder compression equations. Powder. Technol. **4**, 61–68 (1971). https://doi.org/10.1016/0032-5910(71)80001-3
30. Huang, P.Y.: Powder Metallurgy Principle. Metallurgical Industry Press, Beijing (2004)
31. Gerde, E., Marder, M.: Friction and fracture. Nature **413**, 285–288 (2001). https://doi.org/10.1038/35095018
32. Azéma, E., Radjaï, F.: Force chains and contact network topology in sheared packings of elongated particles. Phys. Rev. E. **85**, 031303 (2012). https://doi.org/10.1103/PhysRevE.85.031303
33. Sun, Q.C., Jin, F., Liu, J.G.: Understanding force chains in dense granular materials. Int. J. Mod. Phys. B. **24**, 5743–5759 (2010). https://doi.org/10.1142/S0217979210055780
34. Iikawa, N., Bandi, M.M., Katsuragi, H.: Sensitivity of granular force chain orientation to disorder-induced metastable relaxation. Phys. Rev. Lett. **116**, 128001 (2016). https://doi.org/10.1103/PhysRevLett.116.128001
35. Solimanjad, N., Larsson, R.: Die wall friction and influence of some process parameters on friction in iron powder compaction. Mater. Sci. Tech-Lond. **19**, 1777–1782 (2003). https://doi.org/10.1179/026708303225009517
36. Alzouma, O.M., Robisson, A.C.: Die wall lubrication for UO_2 pellets pressing: a case study. Ceram. Int. **44**, 15905–15911 (2018). https://doi.org/10.1016/j.ceramint.2018.06.007